Regular article

Kristjan Leosson*, Arni S. Ingason, Bjorn Agnarsson, Anna Kossoy, Sveinn Olafsson and Malte C. Gather

Ultra-thin gold films on transparent polymers

Abstract: Fabrication of continuous ultra-thin gold films (<10 nm) on the surface of optical polymers (CYCLOTENE and ORMOCLEAR) is reported. Using a range of electrical, optical and structural characterization techniques, we show that polymers can be superior to more conventional (inorganic) materials as optical substrates for realizing ultra-thin gold films. Using these transparent polymer substrates, smooth, patternable gold films can be fabricated with conventional deposition techniques at room temperature, without adhesion or seeding layers, facilitating new photonic and plasmonic nanostructures, including transparent electrical contacts, thin film waveguides, metamaterials, biosensors and high-contrast superlenses.

Keywords: optical polymers; surface plasmons; thin metal films; transparent electrodes; X-ray analysis.

***Corresponding author: Kristjan Leosson,** Science Institute, University of Iceland, Dunhagi 3, IS107 Reykjavik, Iceland, e-mail: kleos@hi.is
Arni S. Ingason: Thin Film Physics, Department of Physics (IFM), Linköping University, SE-581 83 Linköping, Sweden
Bjorn Agnarsson: Department of Applied Physics, Chalmers University of Technology, SE-41296 Gothenburg, Sweden
Anna Kossoy and Sveinn Olafsson: Science Institute, University of Iceland, Dunhagi 3, IS107 Reykjavik, Iceland
Malte C. Gather: Institut für Angewandte Photophysik, TU Dresden, 01062 Dresden, Germany

Edited by Frank Koppens

1 Introduction

A well-known phenomenon in the fabrication of structures and devices involving thin gold films is the formation of three-dimensional islands at the initial stages of film growth, driven mainly by the low surface adhesion of the metal [1]. This self-assembly of isolated nano-scale islands is frequently exploited for practical purposes as it provides a simple way of realizing nanostructured surfaces, suitable for a range of technical applications and fundamental studies [2–6]. As the metal deposition thickness is increased, individual islands grow in size and subsequently partly coalesce to form electrically isolated fractal clusters. Significant changes occur in the optical [4] and electrodynamic [7] properties of the film at this stage and up to the percolation threshold, where deposition thickness has been increased to the point where an electrically conductive path is formed through the network of gold clusters. When additional material is deposited, voids in the percolating network gradually fill up and the film eventually becomes structurally continuous. Unfortunately, in cases where it is desirable to utilize the properties of thin, smooth, continuous metal films on dielectric substrates, this mode of film formation is directly detrimental. Structural imperfections lead to, e.g., increased optical absorption over a wide range of wavelengths due to excitation of localized plasmon resonances, increased scattering in surface plasmon polariton waveguides, decreased imaging contrast in plasmon-assisted superlens lithography [8], as well as increased electrical resistance due to film discontinuity and non-specular reflection of electrons [9].

Gold is a particularly important material for many applications in optics, electronics, photonics, plasmonics, biosensing, and chemical catalysis, as it possesses a number of favorable electrical, optical, physical and chemical properties [10–12]. Fabrication of structurally continuous gold films below 15–20 nm is, in general, difficult to achieve on commonly used optical surfaces, including amorphous and crystalline materials such as glass [13], native silicon oxide [14], Si_3N_4 [15], TiO_2 [16], and certain transparent polymers [17]. For a range of crystalline substrates, including sapphire, mica, silicon, NaCl , KCl, and LiF [9, 11, 18, 19], epitaxial single-crystal gold islands or sheets can be formed. However, these substrates and the required deposition methods are in most cases incompatible with the fabrication of optical or electronic multilayer devices, as they typically require special conditions such as in-situ cleaving, UHV and high-temperature substrate surface reconstruction, elevated deposition temperatures, seeding layers of different chemical species and/or template stripping. In an interesting recent development, (3-mercaptopropyl)trimethoxysilane molecular linkers were shown to improve adhesion of gold to glass [20], but

to our knowledge the wetting characteristics of gold in the thin-film limit on such surfaces has not yet been explored.

One important area where ultra-thin metal films are of great technical interest is in light-emitting and light-harvesting devices. Finding suitable materials to replace the ubiquitous indium tin oxide (ITO) transparent electrodes in such devices remains an important task, particularly for fabrication of flexible organic devices, where ITO's brittleness, high-temperature processing and rising cost are limiting factors. Alternatives presently under consideration include conductive polymers, graphene, metal-polymer nanocomposites, and various types of nanowires or metal film grids [21–24]. Metal films are especially promising due to their potentially high conductivity and large-area, low-temperature processing, with gold being particularly attractive due to its chemical stability and large atomic mass (electromigration resistance). In the context of organic LEDs and solar cells, the high work function of gold ensures efficient hole-injection if gold is used as the anode of these devices. Conversely, if ultra-thin gold films were to be used as cathodes, n-type doping could facilitate electron injection into the organic semiconductor. The tendency of island formation, however, increases sheet resistance and residual optical absorption in certain metal films, as the film thickness is decreased [25].

In the present paper, we report on the fabrication of ultra-thin gold films on two types of commercially available transparent optical polymers, CYCLOTENE3022 (DOW Chemical Co.) and ORMOCLEAR (micro resist technology GmbH). The gold films were fabricated using standard vacuum deposition methods at room temperature without the use of seeding layers. The resulting films show substantially lower coalescence and continuity thresholds than films deposited on, e.g., SiO_2, as revealed by electrical resistance measurements and scanning electron microscopy. Furthermore, X-ray reflection and diffraction measurements reveal clear differences in film formation, with high-density gold films being formed on the polymer surface already at a deposition thickness below 2 nm. Importantly, thin (<20 nm) film patterns can be realized on the polymer substrates using a conventional lift-off process, without the use of adhesion layers that often limit optical performance [26, 27]. As noted above, these results have important implications for thin-film electronics, fabrication of transparent gold contacts, biosensing, metamaterials, plasmonic superlenses, and optical antennas. Furthermore, in the case of plasmonic waveguides, ultra-thin gold films are important in devices utilizing symmetric and anti-symmetric coupled-SPP modes, i.e., the low-loss long-range mode [28, 29] or the highly confined short-range plasmon mode [30, 31]. In particular, the short-range mode is interesting from the point of view of slow light propagation, extreme field confinement and strong light-matter interaction [28, 30]. Finally, the polymer surface layers and deposition methods used in the present study are compatible with "flexible plasmonics" [32] that offers a range of new optical functionalities.

2 Materials and methods

We fabricated gold-coated samples using conventional e-beam (7.5 kV) deposition on a range of differently treated substrates. Control samples fabricated using thermal deposition and DC sputter deposition gave comparable results when characterized by X-ray reflectivity, atomic force microscopy (AFM), or plasmon propagation (see below). As substrates, we used silicon (Si(100) with ≈1.5 nm native oxide), thermally oxidized silicon (100-nm oxide thickness) and borosilicate glass, as well as silicon and glass substrates coated with CYCLOTENE™-3000 polymer (DOW Chemical Co.), commonly referred to as BCB, or the organic-inorganic hybrid ORMOCER®-material ORMOCLEAR (micro resist technology GmbH). CYCLOTENE™ polymers (derived from B-staged bisbenzocyclobutene-based monomers) and ORMOCER® materials (ORganically MOdified CERamics, fabricated by stepwise sol-gel synthesis of inorganic and organic networks) are commonly used as interlayer dielectrics and/or for fabrication of optical devices, including plasmonic devices, and details of their chemical, physical and optical properties have been previously published [33–39]. Both classes of materials can be spin-coated in a wide range of thicknesses, exhibit high transparency, good planarization properties and chemical inertness, which makes them compatible with lithography and lift-off processes involving organic solvents, as well as direct UV patterning and/or dry-etching processes. Partly or fully cured BCB has a relatively large surface energy of 48–50 mJ/m^2 [40], compared to other polymer materials, while reported surface energy values for ORMOCER materials (35–43 mJ/m^2 [41]) are similar to those of many common polymers (including PE, PS, PVC, PMMA, PC, PEEK).

Gold deposition rate was monitored using a quartz-crystal microbalance (QCM) detector and maintained at approximately 0.6 Å/s at a base pressure of 3×10^{-6} mbar. Samples were mounted on a rotating holder, 350 mm above the gold crucible, and placed symmetrically around the rotation axis in order to ensure that the deposited thickness was the same on each sample in a given batch. Up to six different substrates were coated simultaneously

to minimize run-to-run variations. The amount of material ("mass-equivalent thickness") deposited on the samples was determined accurately using the combined results of X-ray reflection, atomic-force microscopy and optical transmission measurements, correlated with the QCM measurements. Gold films were characterized using measurements of X-ray reflectivity and diffraction, electrical conductivity, optical transmission and plasmon propagation, in addition to scanning electron microscopy, as described in more detail below.

3 Results and discussion

3.1 Electrical resistance measurements

Electrical resistance of thin gold films on different substrates was measured with a Keithley 2100 multimeter between 100-nm thick gold contacts patterned by photolithography prior to deposition. Resistance measurements on each sample were repeated at regular intervals over 1 week following the deposition, during which time the samples were kept under ambient conditions in a cleanroom environment. Sheet resistance values of gold films deposited on thermally oxidized or polymer-coated silicon samples are shown in Figure 1. The data points in Figure 1(A) correspond to the film resistance measured 1 week after deposition. Gold deposited on SiO_2 exhibits coalescence (electrical conductivity) at a mass-equivalent thickness of d=6 nm, in agreement with previous reports, e.g., Ref. [7]. Gold deposited on BCB or ORMOCLEAR, on the other hand, changes from an electrically discontinuous to a conducting film at 3–4 nm of mass-equivalent thickness. Furthermore, in the interval 6–10 nm, the sheet resistance of films deposited on polymer coated samples remains a factor of 2–5 lower than that of Au on SiO_2. Film continuity, defined as the minimum of the Rd^2 curve, where R is the sheet resistance [42, 43], occurs at around 8 nm for Au on BCB or ORMOCLEAR, compared to 12 nm for Au on SiO_2. In Figure 1(A) we show, for comparison, room-temperature sheet resistance values extrapolated from low-temperature (4–250 K) data on gold films grown epitaxially with a niobium seeding layer in ultra-high vacuum on high-temperature annealed (1100°C) sapphire substrates [44].

Most samples showed a measurable change in resistance for days after deposition, although the most rapid changes generally took place within the first hour. A steady *decrease* in film resistance (10–20%) was observed during the first week after deposition for continuous films on BCB (d>=3.6 nm), as shown in Figure 1(B). This indicates an improvement in film quality with time through lateral grain growth, similar to what has been observed at room temperature in continuous Au films deposited on SiO_2 [45]. Resistance decreased by a further 20–30% upon annealing the films at 150°C for 1 h. For films below the coalescence threshold on BCB, however, resistance *increased* by 1–2 orders of magnitude within 1 week at room temperature, suggesting that formation of electrically isolated but

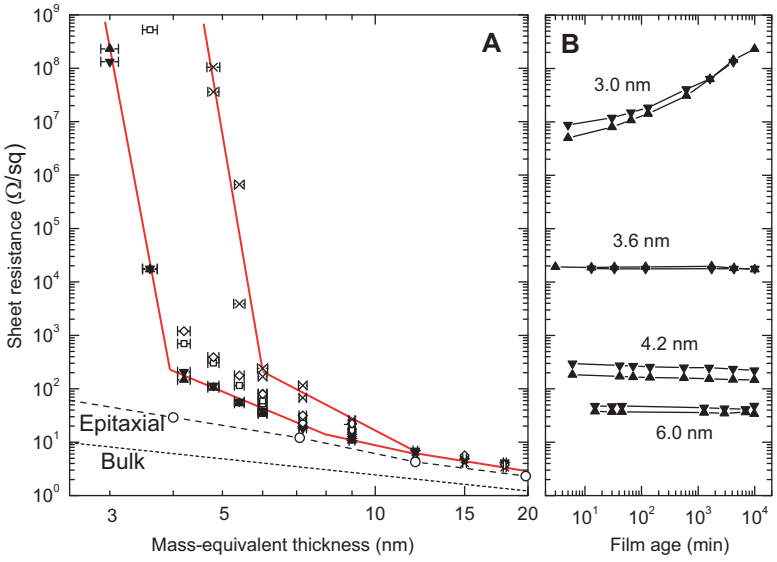

Figure 1 (A) Sheet resistance of gold films deposited onto Si substrates covered with (▼) 100-nm thick BCB, (▲) 10-μm thick BCB, (◊) 300-nm thick ORMOCLEAR (□) 15-μm thick ORMOCLEAR and (×) 100-nm thick SiO_2, all points measured 1 week after deposition. Solid lines are provided as guides to the eye. The resistance of an ideal film with bulk properties is shown with the dotted line. Experimental results (–O–) from epitaxial gold film on sapphire (room temperature values extrapolated from the low-temperature data of Ref. [35]) are also included. (B) Evolution of film resistance after deposition for Au on BCB. Film quality increases with time for >=3.6 nm thickness.

highly compact (see below) gold clusters is thermodynamically preferred at a deposition thickness of 2–3 nm.

3.2 Scanning electron microscopy

Results of the resistance measurements are qualitatively supported by the scanning electron micrographs shown in Figure 2. SEM images were obtained with a Zeiss Supra 25 scanning electron microscope, using an in-lens secondary electron detector, 10 kV acceleration voltage and approximately 1.5 mm working distance. Gold films deposited on SiO_2 exhibit the typical characteristic structure, with electrically isolated islands or clusters up to $d \approx 6$ nm. Gold on BCB polymer, by comparison, forms smaller and more densely packed islands up to $d \approx 3$ nm that coalesce at $d \approx 3$–4 nm. At $d \approx 7$ nm, gold on BCB appears featureless while gold on SiO_2 remains highly structured. Similar behavior was observed for gold on ORMOCLEAR-coated substrates. Equal film thickness was measured in the limit of continuous (15–18 nm) films deposited simultaneously on polymer and glass substrates, suggesting that the sticking probability of gold during initial stages of film formation is comparable. Hence, we propose that the molecular-scale structure of the polymer surface results in an increased number of nucleation sites and reduced surface diffusion of gold atoms, strongly affecting the dynamics of initial film formation. We note, however, that this is not a general rule for polymers, as very different results were obtained for gold films, e.g., on fluoropolymers in Ref. [17].

3.3 X-ray characterization

In order to quantify the thickness, density, roughness and crystallinity of the deposited films, we used X-ray reflection (XRR) and diffraction (XRD) measurements. X-ray analysis was carried out using a Panalytical X'Pert MRD (wavelength 0.15406 nm) equipped with a hybrid monochromator/mirror on the incident side and a 0.27° collimator on the diffracted side. Reflectivity scans were performed with a collimator slit while for high-angle 2θ-ω measurements, the slit was removed. X-ray reflection spectra were fitted with Panalytical Reflectivity software using the Parratt formalism [46] and values of effective film density, effective thickness and roughness of the deposited films were extracted. The fitting model included a thin (approx. 1 nm), variable-density interface layer between the gold and the dielectric, accounting for the possibility of atomic-scale surface roughness and diffusion of gold into the substrate layer. Example fits to XRR curves are shown in Figure 3(A). Effective film density parameters from the fits are shown in Figure 3(B), illustrating a remarkable difference in film growth between the SiO_2 and the polymer surfaces. The effective density of the gold film on SiO_2 drops monotonically with reduced deposition thickness, consistent with the decreasing surface coverage of isolated islands. In contrast, gold on BCB-coated substrates shows a density corresponding to (95±4) % of the bulk density of gold already at a deposition thickness of 2 nm. Gold on ORMOCLEAR exhibits similar behavior but lower effective density, which correlates well with the observed difference in sheet resistance shown in Figure 1(A). The gold film roughness, determined from XRR fits, was measured as (1.0±0.1 nm) for BCB and (1.2±0.1 nm) for ORMOCLEAR across the measured thickness range. For continuous gold films on SiO_2 (>12 nm), however, film roughness determined from the XRR was substantially higher at (2.0±0.1 nm). Changes in the growth dynamics at the initial stages of film formation clearly affect the overall morphology of the gold films, as a reduction in grain size and a smaller degree of texturing in the (111)-direction for gold films on the polymer surface was

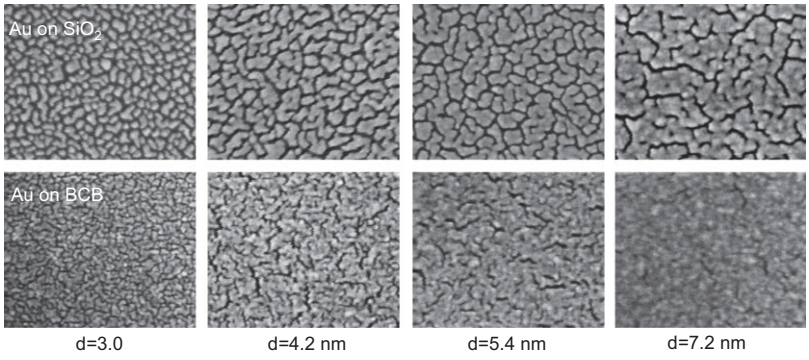

Figure 2 SEM images of gold films on SiO_2 (top row) and BCB polymer (bottom row) at different deposition thickness. All images are 300 nm across.

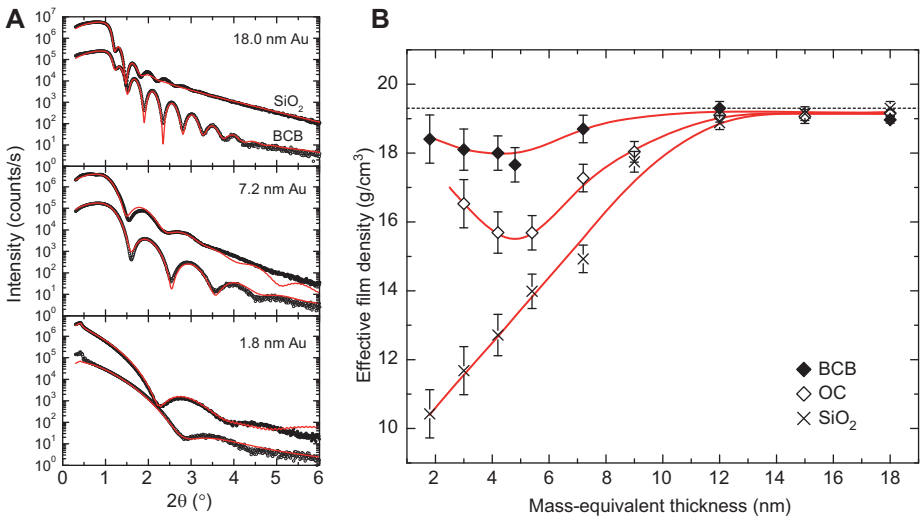

Figure 3 (A) X-ray reflection spectra (black symbols) and corresponding fits (red solid curves). XRR data on thin gold films deposited on BCB consistently reveals better film quality, as compared to gold deposited on SiO_2, as evidenced by lower effective film thickness, higher density and decreased surface roughness (better interference visibility) for identical deposition conditions. The SiO_2 curves have been shifted upwards (5×) for clarity. (b) Film mass density obtained by fitting series of XRR spectra for gold films on (♦) BCB (◊) ORMOCLEAR and (×) SiO_2. Red solid lines are a guide to the eye and the dashed line indicates the bulk density of gold. Letters A mark the onset of coalescence, and letters B designate the points of film continuity. Vertical error bars correspond to the uncertainty in fitting parameters, while uncertainty in thickness is similar to the symbol size.

consistently observed in conventional symmetric 2θ-ω X-ray scans. The initial stages of film formation (0–3 nm deposition thickness) on differently treated surfaces will be described in more detail in a separate publication.

3.4 Optical transmission

Figure 4 compares optical transmission through gold films deposited on Ar/O_2-plasma-cleaned borosilicate glass substrates to transmission through films deposited on BCB-coated glass. Optical transmission spectra were recorded using a collimated white light source (halogen bulb). Light transmitted at normal incidence was collected by an Acton SpectraPro SP-2356 spectrometer, equipped with a CCD camera, using a 150 lines/mm grating. All experimental and theoretical curves include a ≈4% reduction in transmission due to reflection from the backside of the substrate. A (hypothetical) featureless gold film characterized by the bulk dielectric function of bulk gold (from Ref. [47]) has a maximum transmission in the 500–700 nm range, as shown in Figure 4, well matched to visible-wavelength emitters. The bulk dielectric function of polycrystalline gold depends on the grain size of the material and can therefore depend on the method of fabrication and subsequent thermal treatment. In Ref. [47], Johnson and Christy did not observe a change in the dielectric function of continuous gold films (>25 nm) upon annealing (at 150°C), while in a recent publication, Tinguely et al. [48] report a change in both real and imaginary parts of the dielectric function upon annealing (at 200°C), which was attributed to grain growth. It is possible to maintain (as is frequently done in the literature) that the dielectric function of the thin gold layer is also modified by the structure of the film itself (this is sometimes referred to as the "pseudo dielectric function") [49] and even non-local effects in the thin film limit [50]. In order to simplify the discussion, however, we choose here to compare experimentally determined optical transmission to that of a perfectly uniform film, characterized only by the film thickness and the bulk dielectric function of Ref. [47]. Experimentally observed reduction in optical transmission, as compared to this ideal behavior, will therefore be referred to as structure-related "extinction", rather than using the concept of a "dielectric function of the thin film" which we find misleading as it depends on the substrate in question, film thickness, film age, etc. The exact bulk and microstructural contributions to the dielectric response of ultrathin films deposited on different transparent substrates will be discussed elsewhere.

For gold deposited on glass, residual extinction (related mainly to excitation of localized surface plasmons in isolated gold islands) is clearly seen, with the extinction wavelength shifting from 620 nm to 775 nm as the deposition thickness varies from 3 nm to 7 nm. The extinction is most pronounced close to the percolation edge (6 nm),

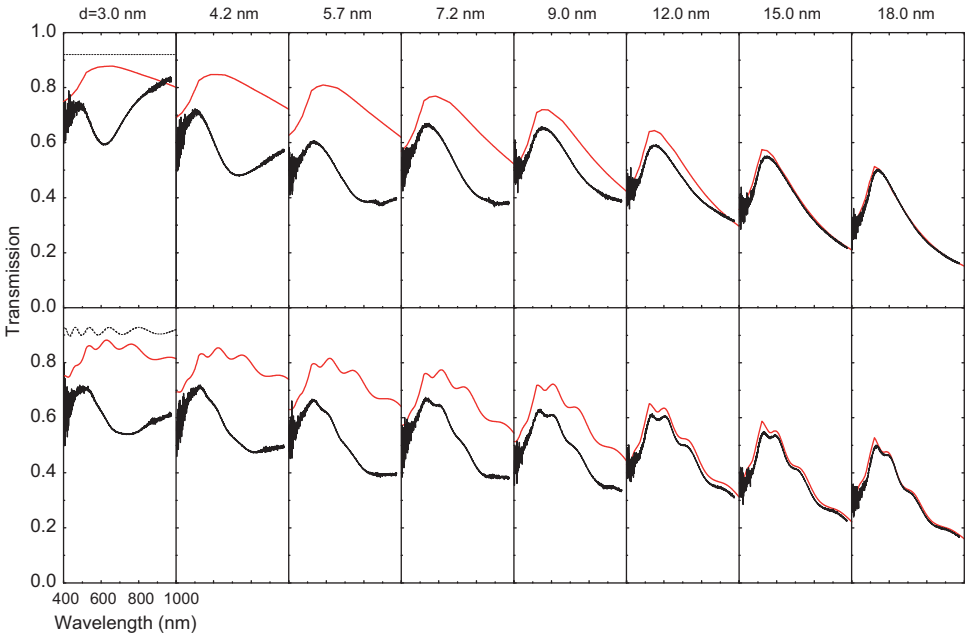

Figure 4 Measured (black lines) and calculated (red lines) optical transmission spectra through gold-coated glass plates. Thin gold films were deposited directly on borosilicate glass (top row) or on BCB-coated glass plates (bottom row). The thickness of the BCB layer in the latter case was 1.0 µm. The leftmost panels also show the calculated transmission without the gold layer (dotted lines). Transmission through films below 15 nm thickness is reduced by residual extinction, as discussed in the text.

consistent with the diverging density of optical states [4]. Glass plates coated with 1.0-µm thick BCB prior to gold deposition also show some residual extinction. However, in this case, the extinction maximum does not shift with increasing deposition thickness, but stays approximately fixed at a wavelength of 765±10 nm for all measured thicknesses, revealing a clear difference in the development of film morphology. On BCB, residual extinction decreases monotonically in magnitude for gold deposition thickness above 3 nm. Glass plates with conductive (<100 Ω/sq) 4.2-nm thick gold films deposited on BCB experimentally show >70% (internal) transmission in the 470–570 nm range. Similar transmission values have been reported for 250°C-annealed gold layers on soda glass [51], but with three orders of magnitude larger sheet resistance. Optical transmission in the visible range is, however, highly sensitive to the structural quality of the gold film and further improvement is still needed to move closer to the theoretical transmission limit (80–90% transmission for 490–850 nm at <100 Ω/sq).

3.5 Surface plasmon polariton propagation

As a final independent check of the film quality, we fabricated thin-film plasmonic stripe waveguides with thicknesses in the range 4–15 nm, embedded in a uniform cladding environment (ORMOCLEAR). Such films support a long-range surface plasmon polariton (LRSPP) mode where propagation loss is expected to decrease rapidly with decreasing metal thickness [52]. For measurements of plasmon propagation, the LRSPP stripe waveguide mode was excited directly by coupling from a polarization-maintaining optical fiber. Coupling was optimized by monitoring the waveguide output and propagation loss was measured by imaging scattered light emitted perpendicular to the sample surface with a CCD camera, and measuring scattered light intensity as a function of position along the waveguide for different wavelengths. Net plasmon amplification at 600 nm wavelength was observed in similar ultra-thin low-loss gold slab waveguides in Ref. [28]. Low surface roughness (≈1 nm or below) on lithographically patterned ultra-thin gold stripes on ORMOCLEAR was confirmed by contact-mode AFM measurements. Figure 5(B) shows results of propagation loss measurements, confirming that propagation loss steadily decreases as the film thickness is reduced. The deviation from theoretically expected values of the propagation loss on an infinite film are partly accounted for by scattering loss originating from the edges of the waveguide, confirmed by the fact that we observed an increase in propagation loss as stripe width was decreased, which is contrary to theoretical expectation if effects of edge scattering are not taken into account [52].

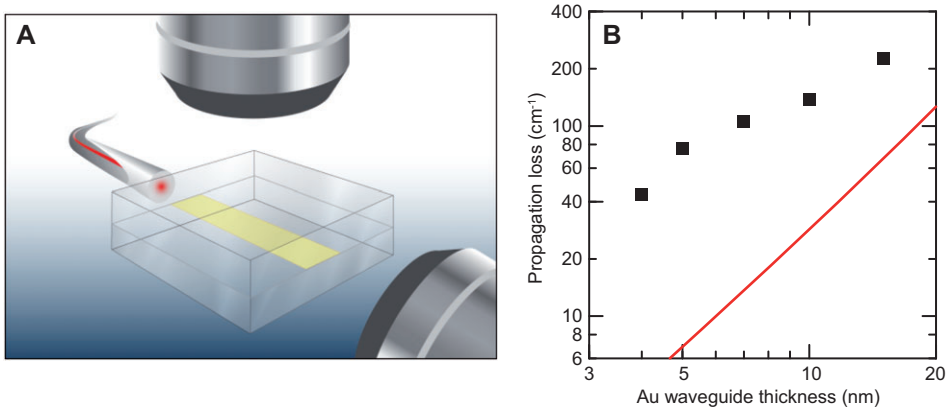

Figure 5 (A) Schematic illustration of the experimental setup for measuring propagation loss in ultra-thin metal stripe waveguides. (B) Measured propagation loss (squares) for 3.5-μm wide gold stripe waveguides embedded in a 30-μm thick ORMOCLEAR cladding, measured at 680 nm free-space wavelength. The solid line shows the theoretical expectation for an ideal planar gold film having a dielectric constant corresponding to bulk material.

4 Conclusions

We have shown that the dynamics of gold film formation on the surface of certain optical polymers can be dramatically different from that on inorganic substrates. The possibility of fabricating and patterning high-mass-density, low-roughness gold films as thin as 2 nm has interesting implications for electronics, optics, photonics, biosensing and surface chemistry. The high structural quality of the ultra-thin metal films, combined with the large effective-index variations that can be introduced through very small metal thickness modulation, translates into a high degree of control over device structure and optical properties. At 4.2 nm deposition thickness, we measured maximum internal transmission of 75% at 530 nm wavelength, in films with sheet resistance as low as 86 Ω/sq. In order to compete with existing transparent contact technologies, further improvement in film quality is necessary to reduce structure-related residual extinction.

The authors recognize that a full understanding of the wetting chemistry of gold on different polymer surfaces can only be obtained using surface characterization methods such as X-ray photoelectron spectroscopy. We plan to pursue such studies in future work. Furthermore, the wide range of possibilities in engineering polymer surface properties should be explored in detail in order to map out and understand nucleation and growth of ultra-thin noble metal films on such surfaces, in order to aid future research and development in plasmonics, metamaterials, light-emitting and light-harvesting devices, and related fields.

Acknowledgements: The research has been supported by the Icelandic Research Fund, grants no. 110004021, 70021021 and 100019011. The authors would like to thank Frimann Kjerulf, Dadi Bjarnason, Gudmundur K. Stefansson, Fridrik Magnus and Ilya Slovinsky for assistance with the measurements. Also, we thank Birgir Johannesson and Jon Matthiasson at the Innovation Center Iceland for microscopy expertise.

Received October 1, 2012; accepted November 30, 2012; previously published online December 25, 2012

References

[1] Shao X, Nilius N, Freund HJ. Crossover from two- to three-dimensional gold particle shapes on CaO films of different thicknesses. Phys Rev B 2012;85:115444-1–8.

[2] Merlen A, Gadenne V, Romann J, Chevallier V, Patrone L, Valmalette JC. Surface enhanced Raman spectroscopy of organic molecules deposited on gold sputtered substrates. Nanotechnology 2009;20:1–7.

[3] Hung WH, Aykol M, Valley D, Hou WB, Cronin SB. Plasmon resonant enhancement of carbon monoxide catalysis. Nano Lett 2010;10:1314–18.

[4] Krachmalnicoff V, Castanie E, De Wilde Y, Carminati R. Fluctuations of the local density of states probe localized surface plasmons on disordered metal films. Phys Rev Lett 2010;105:1–4.

[5] Hiruma K, Haraguchi K, Yazawa M, Madokoro Y, Katsuyama T. Nanometre-sized GaAs wires grown by organo-metallic vapour-phase epitaxy. Nanotechnology 2006;17:S369–75.

[6] Tesler AB, Chuntonov L, Karakouz T, Bendikov TA, Haran G, Vaskevich A, Rubinstein I. Tunable localized plasmon transducers prepared by thermal dewetting of percolated evaporated gold films. J Phys Chem C 2011;115:24642–52.

[7] Hovel M, Gompf B, Dressel M. Dielectric properties of ultrathin metal films around the percolation threshold. Phys Rev B 2010;81:1–8.
[8] Liu H, Wang B, Ke L, Deng J, Chum C, Teo S, Shen L, Maier S, Teng J. High aspect subdiffraction-limit photolithography via a silver superlens. Nano Lett 2012;12:1549–54.
[9] Kastle G, Boyen HG, Koslowski B, Plettl A, Weigl F, Ziemann P. Growth of thin, flat, epitaxial (111) oriented gold films on c-cut sapphire. Surf Sci 2002;498:168–74.
[10] Tassin P, Koschny T, Kafesaki M, Soukoulis CM. A comparison of graphene, superconductors and metals as conductors for metamaterials and plasmonics. Nature Photonics 2012;6:259–64.
[11] Hugall JT, Finnemore AS, Baumberg JJ, Steiner U, Mahajan S. Solvent-Resistant ultraflat gold using liquid glass. Langmuir 2012;28:1347–50.
[12] Maier SA, Brongersma ML, Kik PG, Meltzer S, Requicha AAG, Atwater HA. Plasmonics – A route to nanoscale optical devices. Adv Mater 2001;13:1501–5.
[13] Shon Y-S, Choi HY, Guerrero MS, Kwon C. Preparation of nanostructured film arrays for transmission localized surface plasmon sensing. Plasmonics 2009;4:95–105.
[14] Walther M, Cooke DG, Sherstan C, Hajar M, Freeman MR, Hegmann FA. Terahertz conductivity of thin gold films at the metal-insulator percolation transition. Phys Rev B 2007;76:1–9.
[15] Voss RF, Laibowitz RB, Allessandrini EI. Fractal (Scaling) clusters in thin gold-films near the percolation-threshold. Phys Rev Lett 1982;49:1441–4.
[16] Zhang L, Cosandey F, Persaud R, Madey TE. Initial growth and morphology of thin Au films on TiO2(110). Surf Sci 1999;439:73–85.
[17] Dostalek J, Kasry A, Knoll W. Long range surface plasmons for observation of biomolecular binding events at metallic surfaces. Plasmonics 2007;2:97–106.
[18] Fedotov VA, Uchino T, Ou JY. Low-loss plasmonic metamaterial based on epitaxial gold monocrystal film. Opt Express 2012;20:9545–50.
[19] Piscopiello E, Tapfer L, Antisari MV, Paiano P, Prete P, Lovergine N. Formation of epitaxial gold nanoislands on (100) silicon. Phys Rev B 2008;78:1–7.
[20] Habteyes TG, Dhuey S, Wood E, Gargas D, Cabrini S, Schuck PJ, Alivisatos AP, Leone SR. Metallic adhesion layer induced plasmon damping and molecular linker as a nondamping alternative. Acs Nano 2012;6:5702–9.
[21] Ghosh DS, Chen TL, Pruneri V. High figure-of-merit ultrathin metal transparent electrodes incorporating a conductive grid. Appl Phys Lett 2010;96:1–3.
[22] Kim YH, Sachse C, Machala ML, May C, Muller-Meskamp L, Leo K. Highly conductive PEDOT:PSS electrode with optimized solvent and thermal post-treatment for ITO-Free organic solar cells. Adv Funct Mater 2011;21:1076–81.
[23] Hecht DS, Hu LB, Irvin G. Emerging transparent electrodes based on thin films of carbon nanotubes, Graphene, and metallic nanostructures. Adv Mater 2011;23:1482–1513.
[24] Elbahri M, Hedayati MK, Chakravadhanula VSK, Jamali M, Strunkus T, Zaporojtchenko V, Faupel F. An omnidirectional transparent conducting-metal-based plasmonic nanocomposite. Adv Mater 2011;23:1993–7.
[25] Walzer K, Maennig B, Pfeiffer M, Leo K. Highly efficient organic devices based on electrically doped transport layers. Chem Rev 2007;107:1233–71.
[26] Aouani H, Wenger J, Gerard D, Rigneault H, Devaux E, Ebbesen TW, Mahdavi F, Xu TJ, Blair S. Crucial role of the adhesion layer on the plasmonic fluorescence enhancement. Acs Nano 2009;3:2043–8.
[27] Jiao XJ, Goeckeritz J, Blair S, Oldham M. Localization of Near-Field resonances in bowtie antennae: influence of adhesion layers. Plasmonics 2009;4:37–50.
[28] Gather MC, Meerholz K, Danz N, Leosson K. Net optical gain in a plasmonic waveguide embedded in a fluorescent polymer. Nat Photonics 2010;4:457–61.
[29] Fan H, Buckley R, Berini P. Passive long-range surface plasmon-polariton devices in Cytop. Applied Optics 2012;51:1459–67.
[30] Sondergaard T, Bozhevolnyi S. Slow-plasmon resonant nanostructures: scattering and field enhancements. Phys Rev B 2007;75:073402.
[31] Wan RY, Liu F, Huang YD. Ultrathin layer sensing based on hybrid coupler with short-range surface plasmon polariton and dielectric waveguide. Opt Lett 2010;35:244–6.
[32] Aksu S, Huang M, Artar A, Yanik AA, Selvarasah S, Dokmeci MR, Altug H. Flexible plasmonics on unconventional and nonplanar substrates. Adv Mater 2011;23:4422–30.
[33] Buestrich R, Kahlenberg F, Popall M, Dannberg P, Muller-Fiedler R, Rosch O. ORMOCER (R) s for optical interconnection technology. J Sol-Gel Sci Techn 2001;20:181–6.
[34] Streppel U, Dannberg P, Wachter C, Brauer A, Frohlich L, Houbertz R, Popall M. New wafer-scale fabrication method for stacked optical waveguide interconnects and 3D micro-optic structures using photoresponsive (inorganic-organic hybrid) polymers. Opt Mater 2003;21:475–83.
[35] Reinhardt C, Kiyan R, Passinger S, Stepanov AL, Ostendorf A, Chichkov N. Rapid laser prototyping of plasmonic components. Appl Phys a-Mater 2007;89:321–5.
[36] Haas K-H, Rose K. Hybrid inorganic/organic polymers with nanoscale building blocks: Precursors, processing, properties and applications. Rev Adv Mat Sci 2003;5:47–52.
[37] Kane CF, Krchnavek RR. Benzocyclobutene optical wave-guides. Ieee Photonic Tech L 1995;7:535–7.
[38] Nikolajsen T, Leosson K, Bozhevolnyi SI. Surface plasmon polariton based modulators and switches operating at telecom wavelengths. Appl Phys Lett 2004;85:5833–5.
[39] Reinhardt C, Passinger S, Chichkov BN, Marquart C, Radko IP, Bozhevolnyi SI. Laser-fabricated dielectric optical components for surface plasmon polaritons. Opt Lett 2006;31:1307–9.
[40] McMahon J, Gutmann R, Lu J. Surface energy characterization of partially cured benzocyclobutene for 3D interconnect applications. ECS Transactions 2007;11:421–32.
[41] Uhlig S. ORMOCER materials characterization, LAP-& Micro-Processing: applied to optical interconnects and high-frequency packaging. Linköping: Linköping University; 2006.
[42] Evans BL, Maaroof AI, Xu S. Nucleation and growth of platinum and nickel films on amorphous-carbon substrates. J Appl Phys 1994;76:900–7.
[43] Burgmann FA, Lim SHN, McCulloch DG, Gan BK, Davies KE, McKenzie DR, Bilek MMM. Electrical conductivity as a measure of the continuity of titanium and vanadium thin films. Thin Solid Films 2005;474:341–5.
[44] Kastle G, Boyen HG, Schroder A, Plettl A, Ziemann P. Size effect of the resistivity of thin epitaxial gold films. Phys Rev B 2004;70:165414-1–6.

[45] Wong CC, Smith HI, Thompson CV. Surface-energy-driven secondary grain-growth in thin Au films. Appl Phys Lett 1986;48:335–7.
[46] Parratt LG. Surface studies of solids by total reflection of X-rays. Physical Review 1954;95:359–69.
[47] Johnson PB, Christy RW. Optical constants of the noble metals. Phys Rev B 1972;6:4370–9.
[48] Tinguely J-C, Sow I, Leinar C, Grand J, Hohenau A, Felidj N, Aubard J, Krenn JR. Gold nanoparticles for plasmonic biosensing: the role of metal crystallinity and nanoscale roughness. BioNanoScience 2012;1:128–35.
[49] Fujiwara H. Spectroscopic ellipsometry: principles and applications. Chichester, UK: John Wiley & Sons, Ltd.; 2007:147–207.
[50] de Abajo FJG. Nonlocal effects in the plasmons of strongly interacting nanoparticles, dimers, and waveguides. J Phys Chem C 2008;112:17983–7.
[51] Khan MSR, Reza A. Optical and electrical-properties of optimized thin gold-films as top layer of mis solar-cells. Appl Phys a-Mater 1992;54:204–7.
[52] Berini P. Long-range surface plasmon polaritons. Advances in Optics and Photonics 2009;1:484–588.